AIAA JOURNAL
Vol. 44, No. 11, November 2006

Design Optimization of a Two-Dimensional Subsonic Engine Air Intake

N. Hoyle,* N. W. Bressloff,† and A. J. Keane‡
University of Southampton, Southampton, SO17 1BJ England, United Kingdom

DOI: 10.2514/1.16123

A novel geometry modeling technique is defined for the optimization of pressure recovery through a two-dimensional subsonic diffuser based on that of a Formula One race car airbox. The airbox design procedure involves considering the expansion of the flow entering the airbox coupled with a bend through 90 deg. Both of these features are discussed separately in terms of parameterization approaches before the most suitable techniques are united in the final optimization study producing an airbox harboring strong local geometric control and with a set of design variables compact enough to retain optimizer efficiency. A global Krig response surface model is employed to support our optimization studies, comprising design of experiments and updates based upon the expected improvement to the objective function followed by a local exploration in a reduced area of the design space. We find that we can efficiently converge to an optimum airbox design. The geometry modeling technique discussed allows for potentially radical designs with high pressure recoveries.

Nomenclature

A	=	two-dimensional diffuser width, m
a	=	Hicks–Henne bump amplitude, m
C_p	=	static pressure coefficient
E	=	two-dimensional diffuser total expansion ratio, A_e/A_{in}
$E(x)$	=	local expansion ratio, $A(x)/A_{\text{in}}$
f	=	objective function
k	=	number of dimensions
N	=	diffuser axial length, m
n	=	number of observed responses
p	=	mass-averaged static pressure, Pa
R	=	correlation between two sample points
$\boldsymbol{r}$	=	vector of correlations
T	=	dimensionless width factor of Hicks–Henne bump
U	=	mass-averaged inlet velocity, m/s
$\boldsymbol{x}^*$	=	untried point
x_p	=	normalized distance of Hicks–Henne bump peak along duct centerline from duct entry, $x_p \in [0, 1]$
β	=	wall-contouring parameter
δ_{ij}	=	Kronecker delta where $\delta_{ij} = 1$ if $i = j$ and $\delta_{ij} = 0$ if $i \neq j$
θ, p, λ	=	Kriging hyperparameters
μ	=	mean
$\hat{\mu}$	=	maximum likelihood estimator of the mean
ρ	=	fluid density, kg/m^3
σ^2	=	variance
$\hat{\sigma}^2$	=	maximum likelihood estimator of the variance

Subscripts

in	=	diffuser inlet location
e	=	diffuser exit location measured at the engine filter location

Received 16 February 2005; revision received 5 June 2006; accepted for publication 16 June 2006.

*Ph.D. student, Computational Engineering and Design Research Group.
†Senior Research Fellow, Computational Engineering and Design Research Group.
‡Professor of Computational Engineering, Chair of Computational Engineering and Design Research Group.

I. Introduction

OVER the past century, the design of engine air intakes has played a significant role in both the aerospace and automotive industries as engines have developed in sophistication and performance.

Aircraft intake design requires a steady, high-quality flow into the engine to maintain reliable engine performance through conventional flight to high maneuverability situations.

Automotive intake design seeks to maximize static pressure acting on the intake stroke of the engine cylinders. High static pressure over the cylinders increases the cylinder charge density and hence engine power.

Aerodynamic design for this purpose slowly began to appear on race cars during the first few decades of the 20th century. It was known by this time that diffusers could convert kinetic energy at the diffuser entry into static pressure at the exit but with a low efficiency. Early work started on the improvement of general diffuser efficiency in 1938 [1]. In the cases studied here, we focus on the engine air intakes of race cars, in particular those used in Formula One (F1), namely airboxes. The design of the airbox's geometry, including its bend through 90 deg and the position of the air filter element, all have an impact on cylinder-to-cylinder air distribution and thus engine performance. Hence, aerodynamicists have studied air intakes on F1 race cars since the 1950s. At that time, engines were positioned in front of the driver with a small air vent in the engine cover bodywork over the cylinders. Ten years later, rear-engined cars were introduced in which the engines were left exposed with no covering bodywork. By 1972, the teams had designed large scooplike airboxes sitting above the driver's head. However, safety was increasingly becoming an issue from whence roll bar structures were introduced. Two large scoops either side of the roll bar then became the norm, reducing in size through the early eighties until, in 1989, airboxes appeared akin to those seen today with a single modest-sized entry above the driver's head.

These particular air intakes pose an interesting design challenge. Because of the roll bar specifications and the engine layout configuration [2], they need to expand the flow over a short distance while turning the flow through 90 deg. Presently, F1 teams place a 3-liter V10 engine behind the driver, as seen in Fig. 1 The position of the airbox thus takes advantage of the ramming effects of the oncoming air at high speeds. The exit of the diffuser is located over a trumpet tray at the bottom of which sit an offset array of 10 engine inlet trumpets.

The race car industry relies heavily on the use of computer aided design (CAD). Hence, it is clearly important that our studies use commercially available toolkits within the restraints of an

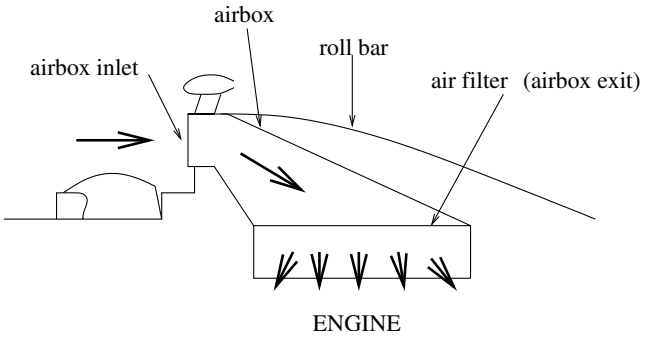

Fig. 1 Airbox positioning within the F1 car.

appropriate amount of compute power, similar to that existing within the race teams of today, to ensure that a realistic solution may be offered. The aim of this paper is to produce a comprehensive study of the design process for a two-dimensional model of the airbox, with special focus on geometric parameterization. Much research has been performed on effectively parameterizing aerofoils by choosing one, or a number of design variables from familiar parameters such as camber, planform, twist, shear, and so on. However, at present there exists no such metric from which we can parameterize an internal flow duct such as an airbox. In this paper, we test a number of simple techniques within an optimization procedure to determine the most effective method for this particular industrial case. Here, optimization is based upon fitting a response surface model (RSM) [3,4] to objective function data generated from CFD simulations at a small number of initial points. A design of experiments (DoE) approach [5] forms the basis upon which these initial points are chosen. The response surfaces created are used to predict objective function values throughout the design space and, consequently, to estimate the position of the optimum. Update points are then chosen from promising regions of the design space, based on the improvement expected to our objective function, so as to increase the accuracy of the response surface fit and, thus, improve the estimated optimum location. For high dimensional problems, it becomes increasingly difficult to perform large numbers of updates due to the computational expense. However, after a reasonable number of update points have been calculated to ensure the current best point is near a promising optimum value, we can perform a local exploration [6] to speed up the convergence and improve the optimum location further to obtain a higher optimum value.

We first discuss geometry parameterization in Sec. II, the design objective in Sec. III and the detail of our CFD model, followed by a further discussion of response surface methodology and local exploration in Sec. IV. In Sec. V, three different geometry parameterizations have been tested for a two-dimensional straight diffuser within an optimization process to determine the most effective method. We investigate the design of two-dimensional elbows of constant width turning through 90 deg in Sec. VI. Again, a variety of simple parameterization methods have been tested for use in optimization. The expansion and bend are then fused together in a novel parameterization method which is employed within the RSM optimization procedure in Sec. VII. This approach has strong local geometric control along the airbox walls allowing the upper and lower wall to be uncoupled. The design variable ranges are chosen such that the geometry also allows for designs with small bumps occurring on the walls. The use of bumps on diffuser walls has been investigated by Zhang et al. [7] and have been seen to be beneficial in reducing pressure distortion over the exit of a curved subsonic S-duct diffuser while maintaining a high pressure recovery.

Following the RSM update process in Sec. VII, a local exploration further enhances the accuracy of the model allowing us to quickly converge to an optimum design. Our approach is successful in producing an efficient optimization strategy with radical results.

II. Geometry Parameterization

Geometry parameterization plays a significant role when used in conjunction with an optimizer. By using a set of variables to define the diffuser in such a way that radical designs are capable of being produced through strong local control on the diffuser walls, the optimizer can discover unconventional designs with the potential to produce superior results. It is clear that using a technique with strong local control is important and our aim is to maximize this control using as small a number of design variables as possible. This will in turn allow us to perform an efficient optimization with the knowledge that our geometry is not overly restricted and thus permitting less intuitive designs.

The literature on geometry parameterization techniques is substantial. Samareh [8] surveyed the available techniques and assessed each on their suitability in dealing with complex models. As we are dealing with curve contours to define the overall geometry of our air intake, we must ensure that these curves are smooth. B-spline and polynomial spline approaches to curve contouring have the advantages of providing a compact set of design variables and are naturally smooth. For simple geometries, Bezier curves are equally as effective with again smooth and accurate properties represented concisely through a small number of design variables. Braibant and Fleury [9] demonstrated that Bezier curves are well suited to geometric parameterization when used in optimization studies and Farin [10] describes some of the more useful properties of this particular technique. Hicks and Henne developed a global shape function to efficiently modify aerofoil sections [11]. Each curve can be smoothly represented through just three design variables: the amplitude of the bump on the curve, the location of the bump on the curve, and the height of the bump. We have applied this technique very effectively to a simple case discussed in Sec. V.

To obtain an understanding of how wall geometry affects the efficiency of expansion and of how the centerline bend affects the efficient turning of the flow, we have initially considered the two functions of the airbox separately: that of expanding the flow through a straight diffuser and that of turning the flow through 90 deg with no expansion. From the conclusions of these studies we choose the best method for parameterizing our airbox, and this is discussed in Sec. VII.

III. Design Objective

Our design problem is the maximization of pressure recovery based on the internal flow through the diffuser. We assume steady, two-dimensional, incompressible flow and so the dimensionless static pressure coefficient, referred to as our pressure recovery value, may be defined by

$$C_p = \frac{p_e - p_{\text{in}}}{q_{\text{in}}} \tag{1}$$

where

$$q_{\text{in}} = \frac{1}{2}\rho U^2 \tag{2}$$

denotes the dynamic pressure.

IV. CFD Analysis and Optimization Strategy

Our geometry is constructed using the CAD engine CATIA V5™ (Dassault Systèmes) and imported into a meshing tool. Both mesh and flow simulations are executed using the commercial CFD package FLUENT [12]. To ensure that solutions yield sufficient accuracy within FLUENT, a mesh dependency study was performed on a straight-walled diffuser before the optimization studies. With a fixed inlet mass flow rate of 10.8 kg/s ($Re = 6 \times 10^6$) and using a paved quad/tri structure for the mesh, various mesh sizes were tested and solved with the same CFD model each time. Starting from a cell count of approximately 1500 cells, the mesh was progressively refined testing approximately 3, 6, 12, 24, 39, 75, and 115 thousand cell meshes. The static pressure recovery value was calculated for each of the different mesh sizes. The percentage difference in C_p value between the meshes comprising approximately 1500 cells and the finest mesh was 437%, whereas the percentage difference in C_p

value between the meshes comprising approximately 39,000 cells and the finest mesh was 1.7%. Hence a mesh with approximately 39,000 cells was chosen for our optimization studies. It is difficult to control the exact cell count when using an automated process to mesh each design discovered by the optimizer such as the one described here. However, the meshes used in this initial dependency study were created with a size function capability within the meshing tool which allows the same growth rate from the boundary layer to be developed regardless of the shape of the diffuser. Using this functionality, finer meshes are produced by decreasing the distance between the mesh nodes on the diffuser walls while maintaining a consistent boundary layer depth across meshes. For cell count consistency within the automation process, the fixed boundary layer depth, fixed distance between wall nodes at the value required to produce an approximately 39,000 cell mesh and a fixed cell growth rate mean that the meshes produced during the optimization process will only vary a small amount in cell count given varying wall shapes.

Our CFD analysis for all the studies carried out in this paper involves solving the two-dimensional steady-state Reynolds-averaged Navier–Stokes equations based on the assumption of two-dimensional steady incompressible flow. The k–ϵ turbulence model [13] is used for our straight diffuser study and our final study in Sec. VII which is in keeping with the references studied, and the Spalart–Allmaras turbulence model [14] is applied in the constant width turning elbow. The change to using a Spalart–Allmaras model is due to the fact that this model is more economic than the standard k–ϵ model and more accurate for wall-bounded flows and flows with mild separation and recirculation [15]. The boundary conditions for studies conducted in Secs. V and VI comprise a fixed mass flow rate of 10.8 kg/s at the inlet and a pressure outflow positioned at the exit of the duct. The exit of the duct is situated downstream of where the engine filter would sit, at the end of the diffuser expansion for the straight diffuser study and at the end of the bend in the elbow study. The end of this constant width extension is classified as the exit. This is to ensure that any separation arising within the diffuser does not pass through the outflow boundary. Mass-averaged static pressure values are taken at the inlet and at the position of the filter for the straight-walled diffuser and at the end of the bend for the elbow.

For the study carried out in Sec. VII, the large expansion required over such a short distance coupled with the 90 deg bend means that a pressure outflow boundary condition at the filter would be insufficient due to the expected unstabilized flow at this point caused by separation. We could extend the diffuser downstream of the filter creating a long constant width outflow duct as carried out in Secs. V and VI, but this is unrealistic in terms of the nature of the airbox set up within an F1 race car. To ensure we obtain accurate converged solutions, we have extended the airbox model to include the engine filter, represented in FLUENT by a one-dimensional porous jump, and the trumpet tray which is an area of fixed width situated between the filter and the engine trumpets. The area represented by the engine trumpets is classified as a velocity inlet boundary condition. A breathing engine sucks the air out of the airbox through the trumpets and so the velocity inlet condition at the trumpets has a negative velocity value. We assume that the four-stroke engine is at wide open throttle running at 18,000 rpm, i.e., we have 9000 intake strokes per minute or 150 intake strokes of the pistons per second. The 3-liter engine requires 0.003 m^3 of air and hence the engine requires a volume flow rate $\dot{V} = 0.45$ m^3/s. This flow rate is also equal to the product of the total cylinder area and the velocity required by the engine. From this the engine velocity can be calculated given the total cylinder area. For the two-dimensional model to be representative of the real 3-D case, the total trumpet length is calculated by matching the 3-D total cylinder area to filter area ratio. However, within the 3-D airbox there is a second expansion ratio of total cylinder area to total inlet area to consider. For this 2-D case, we cannot consider both. Thus, the length of the diffuser inlet and length of the filter are fixed so that the complete shape represents the center plane of a 3-D airbox and the geometry parameterization techniques of defining the walls can be potentially carried over into an airbox design strategy in three dimensions. Then, because our 2-D diffuser is effectively doing half the work needed to expand the flow through a 3-D airbox for the required breathing engine velocity, we need to increase the velocity of the flow being sucked out of the 2-D trumpets to represent sensible inlet speeds akin to those seen in the 3-D case. The velocity through the engine trumpets is such that it is required to have $Re = 2 \times 10^6$. A pressure inlet is imposed at the diffuser inlet. The porous jump values used are given by the thickness and permeability of the engine filters typically used by F1 teams and have the following values: face permeability $= 1.3 \times 10^{-8}$ m^2, filter thickness $= 15$ mm and pressure jump coefficient $= 1000$.

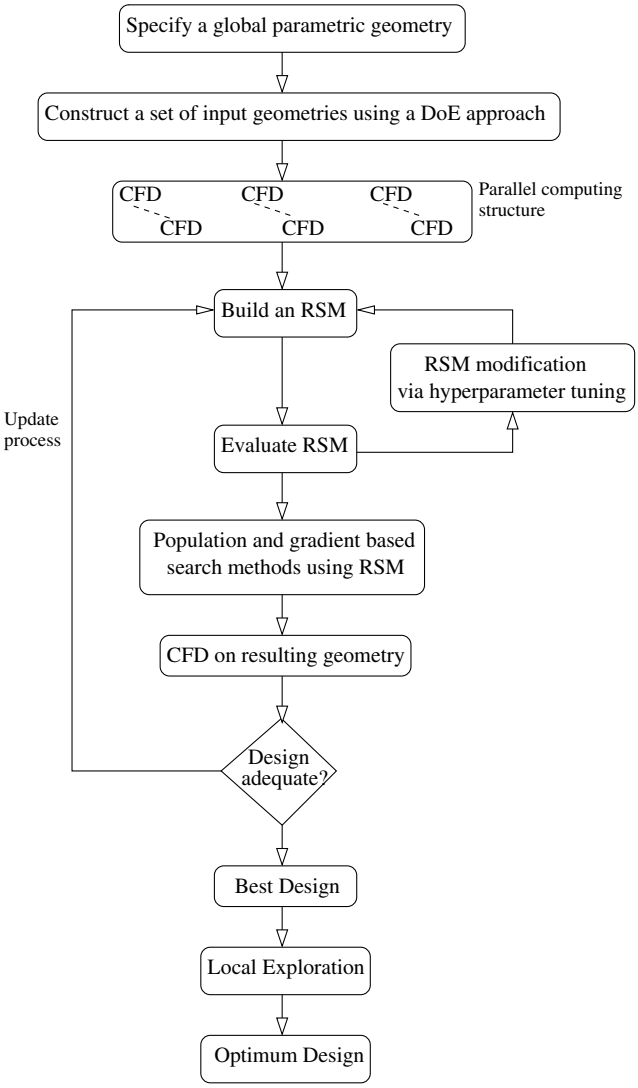

Fig. 2 Typical optimization strategy.

The optimization strategy used in this work is illustrated in Fig. 2. The purpose of this methodology is to conduct a series of CFD evaluations of carefully chosen designs in the search for the optimum design.

A parametric geometry is first specified. Then, a set of design points are created using a DoE [5] approach which supplies the training data for the construction of a response surface model [4] produced in these studies by OPTIONS [16]. This is a form of curve fit through or near the data. Because we do not have any previous knowledge of what this surface looks like, it is considered beneficial to use a technique which provides good coverage of the design space. In our case, we use the LPτ method [17,18]. These points are evaluated using the CFD analysis as described and can be performed within a parallel computing architecture to reduce the computational time required.

A reasonable size DoE should be implemented to build a sufficiently accurate model to initiate the update process. Typically,

10 times the number of design variables is sufficient. For further discussions on this topic refer to Sóbester et al. [19].

A. The Update Process

Having sampled the problem space, a Kriging [20] model is used to construct the RSM [4], see fourth box in flow chart illustrated in Fig. 2. The original purpose of Kriging was to use prior knowledge about the spatial distribution of a mineral which encapsulates the behavior of mineral distribution within the given sample space [21]. Given these sample values and distributions, Kriging can approximately predict the level of mineral concentration at unsampled points. We apply this technique here with the mineral concentration replaced by our objective function, C_p.

Kriging is a technique which provides a statistical interpretation so that, in addition to the predictor, a measure of the possible errors in the model is ascertained, which in turn may be used to position any further design points more prudently. In all cases studied in subsequent sections, the response surface represents an approximation of the expected improvement in the objective function value that can hypothetically be attained over the design space.

We must be aware that Kriging is not suited to all practical applications. Its efficiency is dependent largely upon the number of design variables defining the problem and also the data set size. We have already mentioned in Sec. II that strong local control of the diffuser walls is important. In many cases, local control can be strengthened by adding more points through which splines pass, for example, or control points defining Bezier curves or number of Hicks–Henne functions. This would be deemed useful if we were to be studying an already optimized design and further fine-tuning in specific areas were required. This is not the case for this airbox study and so by potentially enhancing the geometry in terms of its local control strength, the number of design variables, i.e., problem dimension size, increases. Therefore, we face the decision as to whether we can trade off the geometric complexity of the model with the computational time required to obtain an adequate solution. Typically, Kriging is computationally practicable up to approximately 20 design variables [22]. In this paper, we feel it necessary to explore the simplest techniques with small numbers of design variables so that we can compile a parameterization technique for the final study which falls within this 20 design variable limit.

Mathematically, the update process is performed as follows. From the DoE we have a vector of n initial sample points. Each of the n sample points has a response y determined by the objective function $y = f(\boldsymbol{x})$, where in this paper the function f determines the pressure recovery value through the airbox as defined in Sec. III, and $\boldsymbol{x}$ is a vector $(x_1, \ldots, x_k)$ where k denotes the dimension size of the problem. Intuitively, assuming continuity of f, the difference between the responses $y(\boldsymbol{x}_i)$ and $y(\boldsymbol{x}_j)$ will be small if the distance between $\boldsymbol{x}_i$ and $\boldsymbol{x}_j$ is small. This has a statistical interpretation being that $y(\boldsymbol{x}_i)$ and $y(\boldsymbol{x}_j)$ are highly correlated if $\|\boldsymbol{x}_i - \boldsymbol{x}_j\|$ is small. We can express this correlation as

$$R(\boldsymbol{x}_i, \boldsymbol{x}_j) = \exp\left(-\sum_{s=1}^{k} 10^{\theta_s}|x_{is} - x_{js}|^{p_s}\right) + 10^{\lambda}\delta_{ij} \tag{3}$$

satisfying $R = 1 + 10^{\lambda}$ if $\boldsymbol{x}_i = \boldsymbol{x}_j$ and where θ_s, p_s, and λ are unknown coefficients and are defined as the Kriging hyperparameters which provide a good statistical interpretation on the quality of the surface being built and, once tuned, they can be used to rank the design variables in accordance to their relative dominance [22,23].

Now suppose that our set of responses $\boldsymbol{y} = (y_1, y_2, \ldots, y_n)^T$ follows a normal distribution with mean μ and variance σ^2. To estimate the values of μ, σ^2, θ_s, p_s, and λ, we look to choose values for these parameters which will maximize the likelihood of our responses.

The likelihood can be defined as

$$\frac{1}{(\sigma^2)^{n/2}(2\pi)^{n/2}\det \boldsymbol{R}^{1/2}} \exp\left(-\frac{(\boldsymbol{y} - \mathbf{1}\mu)^T \boldsymbol{R}^{-1}(\boldsymbol{y} - \mathbf{1}\mu)}{2\sigma^2}\right) \tag{4}$$

In practice, however, it is more convenient to choose the parameters $\hat{\mu}$ and $\hat{\sigma}^2$ to maximize the log-likelihood function

$$-\frac{n}{2}\log(\sigma^2) - \frac{1}{2}\log(|\boldsymbol{R}|) - \frac{(\boldsymbol{y} - \mathbf{1}\mu)^T \boldsymbol{R}^{-1}(\boldsymbol{y} - \mathbf{1}\mu)}{2\sigma^2} + \text{constant terms} \tag{5}$$

as performed in the "Evaluate RSM" box in Fig. 2.

The maximum likelihood estimators $\hat{\mu}$ and $\hat{\sigma}^2$ of this are then defined by

$$\hat{\mu} = \frac{\mathbf{1}^T \boldsymbol{R}^{-1} \boldsymbol{y}}{\mathbf{1}^T \boldsymbol{R}^{-1} \mathbf{1}} \tag{6}$$

$$\hat{\sigma}^2 = \frac{(\boldsymbol{y} - \mathbf{1}\hat{\mu})^T \boldsymbol{R}^{-1}(\boldsymbol{y} - \mathbf{1}\hat{\mu})}{n} \tag{7}$$

By substituting the values for $\hat{\mu}$ and $\hat{\sigma}^2$ into Eq. (5) we obtain the concentrated log-likelihood function

$$-\frac{n}{2}\log(\hat{\sigma}^2) - \frac{1}{2}\log(|\boldsymbol{R}|) + \text{constant terms} \tag{8}$$

We can maximize this concentrated log-likelihood function to find estimators and $\hat{\lambda}$, $\hat{\theta}_s$, and $\hat{p}_s$, $s = 1, \ldots, k$. This is known as "tuning" the hyperparameters, see Fig. 2, and by doing this we can increase the predictive accuracy of the RSM. Furthermore, we can readily assess the relative dominance of the design variables using the hyperparameters, $\log\theta_s > 0$, $0 < p \leq 2$. For example, a large $\log\theta_s$ value indicates a function whereby the objective value can change significantly over a small distance. p determines the smoothness of the function, the smoother the function the closer to $2p$ gets. For an interpolating model $\lambda = -\infty$, or in practice -6 or less to prevent ill-conditioning of the $\boldsymbol{R}$ matrix. Regression is allowed to occur for values of λ greater than -6.

In Secs. V, VI, and VII we tune the hyperparameters for every 10 update points due to the computational expense incurred by tuning, under the assumption that the character of the surface will remain largely unchanged at intermediate updates.

When exploiting the RSM, we choose a search method to find the best candidate point on the model that maximizes the expected improvement we could achieve over the predicted f values. This occurs in the "Population and gradient based search methods using RSM" box in Fig. 2.

To arrive at a prediction for the objective function at some untried candidate point $\boldsymbol{x}^*$, an objective function value is estimated and augmented to our initial n-dimensional data set. An intuitive predictor of $y^* = y(\boldsymbol{x}^*)$ would be the value which maximizes the augmented log-likelihood function

$$\left[\frac{-1}{2\hat{\sigma}^2(1 - \boldsymbol{r}^T\boldsymbol{R}^{-1}\boldsymbol{r})}\right](y^* - \hat{\mu})^2 + \left[\frac{\boldsymbol{r}^T\boldsymbol{R}^{-1}(\boldsymbol{y} - \mathbf{1}\hat{\mu})}{\hat{\sigma}^2(1 - \boldsymbol{r}^T\boldsymbol{R}^{-1}\boldsymbol{r})}\right](y^* - \hat{\mu}) + \text{terms independent of } y^* \tag{9}$$

for which the maximum of this is our Kriging predictor:

$$\hat{y}(\boldsymbol{x}^*) = \hat{\mu} + \boldsymbol{r}^T\boldsymbol{R}^{-1}(\boldsymbol{y} - \mathbf{1}\hat{\mu}) \tag{10}$$

where $\boldsymbol{r}$ is the vector of correlations $\boldsymbol{r} = [R(\boldsymbol{x}^*, \boldsymbol{x}_1), \ldots, R(\boldsymbol{x}^*, \boldsymbol{x}_n)]^T$.

Expected improvement can be defined as the improvement we can expect to achieve when the model is sampled at an untried point. Let a random variable $Y \sim N[\hat{y}(\boldsymbol{x}), s^2]$ where $\hat{y}$ is our Kriging predictor defined in Eq. (10) and s^2 is our mean square error. For a maximization problem, let $f_{\max}$ be the current best objective function value, then we will achieve an improvement if $I = Y(\boldsymbol{x}) - f_{\max} > 0$.

The expectation of I can be defined as

$$E(I) = \int_{I=0}^{I=\infty} I\left\{\frac{1}{\sqrt{2\pi}s(\boldsymbol{x})}\exp\left[-\frac{[I + f_{\max} - \hat{y}(\boldsymbol{x})]^2}{2s(\boldsymbol{x})^2}\right]\right\} \mathrm{d}I \quad (11)$$

which can be integrated to give

$$E(I) = s[u\,\mathrm{cdf}\,(u) + \mathrm{pdf}\,(u)] \quad (12)$$

where cdf (u) is the normal cumulative distribution function and pdf (u) the normal probability density function and where $u = (\hat{y} - f_{\max})/s$.

This is the value which is searched and maximized using a population based method, the Dynamic Hill Climber [24], to find the next best update point.

This iterative updating process continues until we have an adequate design, i.e., we have obtained a sufficiently high pressure recovery value or we run out of time. Generally, the minimum number of updates needed to yield a convergent solution has been found to be roughly 2–3 times the size of the initial DoE, provided the DoE contains sufficient data for the initial model to be representative [19].

B. Local Exploration

An efficient RSM approach will yield a good global approximation of our objective function. For high dimensionality problems, a large initial DoE is performed but as the number of update points increases, it becomes impracticable to build and tune the RSM using Kriging. Once we have reached the limit of sensible RSM construction times we can move to performing local exploration instead [6]. Provided a reasonable number of update points have been calculated we can ensure that the current best point is near a promising optimum value. We can then perform a local exploration at this point to speed up the convergence upon an optimum value and improve the optimum location further.

Sections V and VI do not contain studies with high dimensionality problems and so their optimization strategies conclude at the "Best Design" box illustrated in Fig. 2. However, the high dimensional problem studied in Sec. VII means that the limit of practical RSM building times is reached and hence the continuation of the strategy into performing a simple local exploration is warranted.

For the combined study, the search of the design space up until this point has been performed within a k-dimensional hypercube defined by the upper and lower bounds of the k design variables. The design space in which the local exploration is performed in this study is fixed in a reduced area of the design space. A small percentage of the design space for each variable is taken around the current best point. We choose this exploration region to be 20% of each of the design variable ranges with the center of this smaller hypercube at the current best point. Within this exploration region we construct a regional set of geometries via a further 50 point LPτ DoE and evaluate these points using the CFD code to obtain their objective function values. No RSM is built using these values as the purpose of this region is to find potentially superior designs through the dense sampling of points within a small area. Efficient local convergence can be assured through this approach.

V. Two-Dimensional Straight Diffuser

Early experimental work classified the major flow regimes within straight diffusers [25,26]. Relationships were deduced between these flow regimes and the diffuser characteristics [27] while, concurrently, a simple geometry parameterization gave room for more efficient designs [28].

Once sufficient computer power became available in the early 1970s, computational design through shape optimization and prediction of fluid flow behavior became feasible. One of the first computational solves of an optimal condition described by mathematical theory was performed by Glowinski and Pironneau [29]. Increased levels of compute power combined with the enhanced efficiency of optimization techniques has enabled us to search larger design spaces and many more designs. Research has been carried out on the optimal shape design of two-dimensional diffusers in turbulent flow using alternative methods to provide an accurate prediction of the flow separation [30,31]. These cases began from a widely studied optimal diffuser design.

As we start with no previous optimized design, we first center our attention on that of a straight diffuser so as to understand the effect of wall geometry on the diffuser. In this section, we consider three different parameterization techniques for diffusers with straight centerlines. Our two-dimensional diffusers have a total expansion ratio $E = 4.5$ and aspect ratio $N/A_{\text{in}} = 1.6$. The flow regimes classified by Fox and Kline [26] established a correlation between diffuser performance and flow separation occurrence for varying expansion ratio and aspect ratio values and given Reynolds number, $Re = 1.6 \times 10^5$. Ideally, to obtain the best possible diffuser performance, the diffuser would be designed so that no areas of separation occurred. This is because separation regions obstruct the effective flow passage and therefore the diffuser would experience increased losses from the excessive nonuniformity of the exit flow. However, if we were to impose a straight wall for our diffuser, the expansion and aspect ratios are such that, referring to Fox and Kline's flow regimes, we would expect to see an inevitable onset of separation. Hence, the purpose of this parameterization exercise within the design optimization strategy is to allow contouring of the wall so that any separation could be reduced or even eliminated given a Reynolds number of 6×10^6.

Wall contouring was first tested for two-dimensional straight diffusers using experimental means by Carlson et al. [28]. It was found that for $E \in [1.5, 4.5]$ and $N/A_{\text{in}} \in [3, 18]$, bell-shaped optimum wall geometries returned the highest C_p value within their optimization study. Madsen et al. [32] studied this problem using CFD and modern optimizer codes, maximizing the static pressure rise, adopting a B-spline parameterization with five master points along the wall. They compared computed results through the use of CFD with those obtained experimentally by Reneau [27] imposing a recreation of the same inlet conditions for a straight-walled diffuser. It was shown that for the straight-walled benchmark diffuser, the CFD code consistently overestimated the pressure recovery values found via experiment, explained by the use of a stationary CFD model where flow separation occurs. However, it was confirmed that with the diffuser geometries falling within the bounds $E \in [1.5, 3]$ with a constant aspect ratio $N/A_{\text{in}} = 3$, Madsen et al.'s parameterization technique coupled with their optimization strategy produced bell-shaped diffusers which were found to return the highest static pressure recovery (C_p values), the same conclusion made by Carlson et al. [28].

With the CFD analyses discussed here we feel it important to validate our CFD model setup with the results obtained computationally by Madsen et al. [32] for the straight-walled diffuser. Therefore, a geometry was created, matching an expansion ratio described in the reference to validate our CFD model setup. It was found that our pressure recovery values converged to within 2% of those in the reference.

A. Geometry Parameterization

1. *Parameterization One: Polynomial Splines*

First we used a model comprising four separate piecewise polynomial splines, referred to from here on as simply splines, that pass through five points along the wall. The advantage of using piecewise splines instead of a continuous cubic spline is that a continuous spline is governed by both C^1 and C^2 continuity at each point. This observation leads us to conclude that this provides less local control of the wall shape than we would ideally like. By demanding the continuity of the second order derivative at each point we are ensuring that at these points, the rate of change of gradient must remain the same. This could lead to the spline "overshooting" the points through which the continuous cubic spline passes and causing a "rippling" effect: a situation that we would wish to avoid.

We define the duct to be symmetrical about its centerline with a cross-sectional area given by

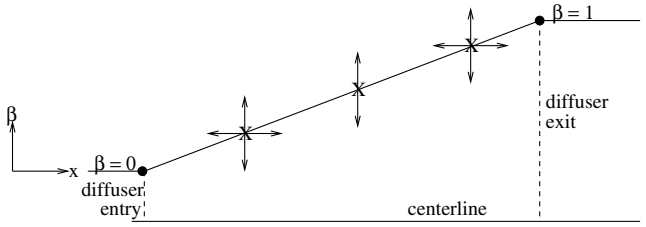

Fig. 3 Spline parameterization of the symmetry half of the straight diffuser.

$$A(x) = A_{\text{in}} + (A_e - A_{\text{in}})\beta(x) \tag{13}$$

where $0 \leq \beta(x) \leq 1$.

The parameter β is varied along the duct by treating it as a function of the x-coordinate of the centerline at that particular cross section. To avoid the problem of rippling through these points by using cubics, we have chosen the first and last splines to be cubic and the middle two to be quadratic curves. This approach means that we are not restricting our problem by having too many constraints over the geometry to maintain continuity at the joints between the curves. Ghate et al. [33] followed this approach to parameterize a duct using three piecewise cubics.

In our case a five-dimensional problem can then be set up as in Fig. 3.

The piecewise variation of β is then prescribed as

$$\beta(x) = \begin{cases} c_{11} + c_{12}x + c_{13}x^2 + c_{14}x^3 & 0 \leq x \leq x_1, \\ c_{21} + c_{22}x + c_{23}x^2 & x_1 \leq x \leq x_2, \\ c_{31} + c_{32}x + c_{33}x^2 & x_2 \leq x \leq x_3, \\ c_{41} + c_{42}x + c_{43}x^2 + c_{44}x^3 & x_3 \leq x \leq x_4 \end{cases} \tag{14}$$

Using the boundary conditions, setting the derivative at the end points to be zero, and the continuity conditions on β we can express the coefficients c_{ij} entirely in terms of $x_1, \ldots, x_5$ and $\beta_1, \ldots, \beta_3$, with the area of each cross section being calculated using Eq. (13).

2. *Parameterizations Two and Three: Hicks–Henne Functions*

A suitable curve can also be modeled using the bump functions introduced by Hicks and Henne [11]. Our second parameterization involves a wall defined via a single Hicks–Henne function. These are global shape functions which allow for good local control and can be written in a general form [34]:

$$f = a[\sin(\pi x^{(-\log 2)/\log x_p})]^T \tag{15}$$

These functions always guarantee smooth curves and also have the appropriate end constraints. Here we superpose the function on a simple straight-sided duct, normalized such that the wall distance $x \in [0, 1]$. Using one of these functions to describe the wall geometry, we have three design variables: a, $x_p \in [0, 1]$, and T.

Finally, our third parameterization involved two Hicks–Henne bump functions summed together to give a total of six design variables. This provides us with further geometries where greater local control of the curve is possible.

B. Results

For our problem, convergent-divergent diffusers began to materialize with competitive C_p values for all of our tested techniques. We found that by converging the flow slightly at the inlet, the acceleration of the flow from the increase in local Reynolds number increases the turbulence of this flow and hence increases the turbulence of the boundary layer. This increase in turbulence is sufficient to prevent the onset of separation. The contours of velocity magnitude in a convergent-divergent diffuser, here found as the optimum via the single Hicks–Henne approach, and in a straight-walled diffuser for comparison, are illustrated at the top and bottom of Fig. 4, respectively. This figure illustrates the whole computational domain of the symmetry half for each. The diffuser section has been magnified to show the difference in geometry. In the

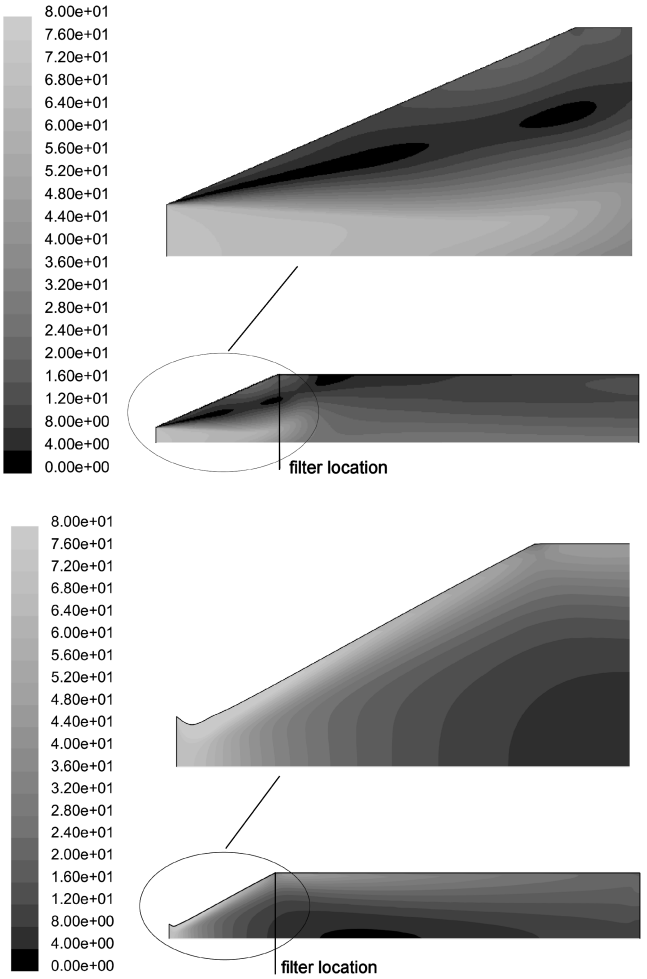

Fig. 4 Filled contours of velocity magnitude in a straight wall and optimum convergent-divergent diffuser.

straight-walled figure at the top, we can see that above the main core of flow, there is an area of recirculation. Here, the flow separated close to the diffuser entry. Because there is a region of high velocity flow and a region of very low velocity flow within the recirculation area at the filter point, the mass-averaged static pressure recovery returns a low overall value of $C_p = 0.21$. In contrast, the flow in the converging-diverging wall diffuser pictured at the bottom of Fig. 4 expands with no separation and has a more even pressure uniformity across the filter. Because of this, the flow is generally at a relatively low velocity through the filter, even with the slight acceleration near the inlet caused by the converging wall, and hence returns a higher mass-averaged static pressure recovery value of $C_p = 0.36$. The optimum diffuser for both the double Hicks–Henne function and the spline technique also yielded a convergent-divergent diffuser almost exactly matching that of the one shown at the bottom of Fig. 4. Essentially we have shown that, given an appropriate optimization strategy in terms of an accurately represented RSM, the varying parameterization techniques tested are capable of producing results with the same geometrical features. We can conclude that given a straight diffusion of flow, we can choose the single Hicks–Henne approach which uses the fewest design variables. However, we feel that for a turning expanding diffuser as studied in Sec. VII, a polynomial spline parameterization would be the appropriate option to pursue for two reasons: first, a single Hicks–Henne function applied upon a straight line connecting the entry to the filter of the airbox would only allow for one bump to contour the shape, whereas the spline technique will be capable of producing a convergence near the entry and a bulge near the exit, for example, giving us a stronger local control of the wall shape; second, constructing spline defined walls is an inbuilt function within the CAD engine used and hence easier to implement from an industrial designer's point of view.

With our inlet speed and expansion conditions, the point of separation occurring within the diffusers studied here are different to those studied by Carlson et al. [28] and Madsen et al. [32]. This explains why none of our three parameterization techniques yielded a bell-shaped optimal design. The physical reasoning behind the bell-shaped designs is that provided the boundary layer is sufficiently turbulent at the inlet, this will ensure that the boundary layer will remain attached during the prime area enlargement. However, our studies show that our flow has too high a velocity, given the expansion required, for the boundary layer to remain attached. Hence, bell-shapes produced poor designs as our flow could not reattach within the specified axial length, where the reattachment occurred between 0.8 and 1.2 m downstream of the filter, resulting in a low C_p value. Because of the fixed engine position and strict overall car dimensions required by the race regulatory bodies, we cannot allow for a longer diffuser to follow the flow streamlines in order for the flow to reattach.

Instead, during the optimization process used here an interesting design began to form. Prior studies such as the five-dimensional case using B-splines tested by Madsen et al. [35] constrained the geometries such that a positive wall slope was seen along the wall. However, considering our different required speed and expansion, we did not stipulate this condition. Although we specified tangency conditions at both the entry and exit points of the diffuser, for the Hicks–Henne defined parameterizations we did not limit the variable bounds such that a negative bump amplitude would be rejected for points placed near the entry point. Although the spline technique limited our wall height variable β to the interval [0, 1], see Fig. 3, the value of β and the position of the first control point coupled with an appropriate β-value for the second control point could lead to a wall shape with a negative wall gradient seen near the inlet.

VI. Two-Dimensional Elbow

Following the study of the preceding section we next consider two different parameterization methods for a duct of constant width turning through 90 deg. The purpose of this study, as in the preceding section, is to determine whether different parameterization schemes offering different numbers of design variables can affect the optimum design output from the same optimization process.

A. Geometry Parameterization

Over the distance within which an F1 diffuser turns, an optimization cycle implemented on a nondiffusing elbow over the same distance would return similar C_p values no matter how the geometric shape varied. This is because the flow would not separate. By shortening the distance over which the elbow bends through 90 deg we can ensure an amount of separation in the poorer designs forcing the optimizer to work harder to find an optimum.

1. Parameterization One: Bezier Curves

Our first curved duct employed a Bezier curve [36] with six overall control points defining the centerline, of which two are considered as variables, see Fig. 5. Two control points are fixed on the inlet and filter position planes and two are placed in a fixed position to impose the tangency condition at the entry and exit to the bend. Two parallel walls were constructed equidistant from the centerline on each side to construct the constant width elbow. Horizontal and vertical tangency conditions were implemented at the entry and exit, respectively, by fixing control points along the required tangency. These conditions prevent designs harboring a sharp point at the diffuser exit onto which the trumpet tray would join.

2. Parameterization Two: Polynomial Splines

The alternative parameterization was set using a cubic spline passing through three points positioned along the centerline. Again, two parallel equidistant walls were placed either side of the centerline. Although we increase our design variable count by two, an advantage of this method over the Bezier curve approach is that continuity conditions are implemented at the entry and exit to the bend without the need of extra fixed control points.

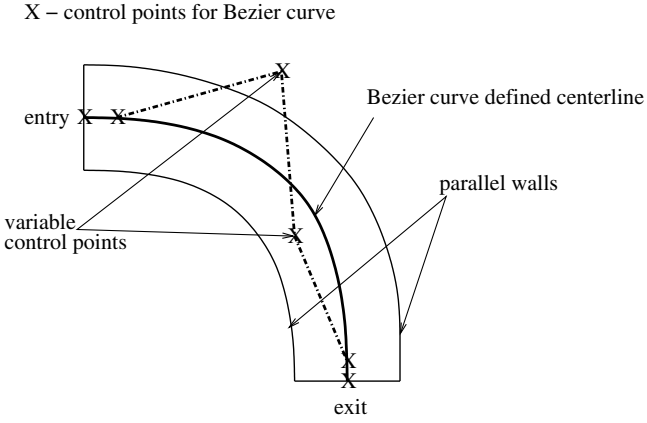

Fig. 5 Geometry parameterization shown for a Bezier curve defined centerline.

B. Results

In this study, all of the designs tested within the optimization process returned a negative pressure recovery. This is because there is no expansion and hence no pressure being recovered due to the reduction of the flow's kinetic energy. So, the static pressure over the filter or exit of the bend is less than the static pressure at which the flow enters the bend. However, both parameterization methods returned similar optimum pressure recoveries of $C_p = -0.0413$ for the Bezier curve method and $C_p = -0.0415$ for the spline method, with similar geometries. These geometries turn the flow through 90 deg and at a gradual and even rate throughout the bend. This ensures that there is no boundary layer separation.

Although both designs produced similar optimum C_p values, in looking forward towards the fusing of the expansion and the bend, the piecewise spline approach appears to be the most efficient when defining the centerline bend. Bezier curves have an inherent problem in that we cannot set a tangency at an end point of the curve without requiring extra fixed control points next to the entry and exit points in the direction of the required tangency through which the Bezier curve must pass. The degree of tangency is then based upon the distance of these extra control points away from the points positioned on the entry and filter planes, which could become extra variables if wanted. This is easily dealt with when using polynomial splines. Given this extra complication within the geometry, we opt to pursue our remaining study with the piecewise cubic spline defined centerline.

VII. Two-Dimensional Diffuser with Bend

A. Combined Geometry Parameterization

The geometric fusion of the expansion and bend parameterizations from the preceding two sections is next used to create a two-dimensional airbox model. It is important to note that to maximize the amount of local control of the overall diffuser shape given to the optimizer, so as to allow the production of potentially radical results, the upper and lower walls need to be completely uncoupled. Thus, the positioning of the control points through which the upper wall spline passes must be independent of the control points defining the lower wall spline. This is ensured by using a model where there are no links between the centerline bend and spline control point positioning variables. This then prevents the problem of wrinkles or loops forming on the lower wall spline leading to geometrically infeasible designs.

The resulting parameterization involves the use of piecewise cubic splines for all three sections. As noted in Sec. V, the most efficient simple expansion materialized as a convergent-divergent diffuser using a polynomial spline parameterization. Hence, here the upper and lower wall variables were left free to produce convergent-divergent diffusers should good C_p values be returned for these

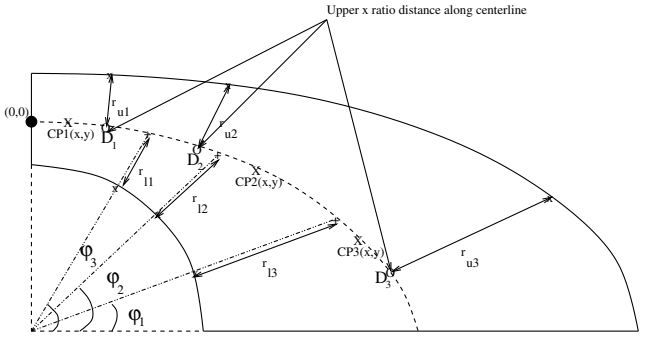

Fig. 6 Geometry parameterization of airbox model.

design points. From Sec. VI it was shown that efficient turning of the flow occurs through a regular and gradual bend and hence the ranges allowed for the three centerline control points are chosen with this in mind. The following parameterization technique for our airbox model features uncoupled walls together with the capability of designs allowing converging walls or walls featuring bumps for example. This technique, with a variable count within the 20 design variable limit, has been devised to give us the potential to produce possibly radical results with good pressure recovery values.

This technique is illustrated in Fig. 6. This requires a total of 16 design variables: six for the centerline control points CP1(x, y), CP2(x, y), CP3(x, y); five for the upper wall r_{u1}, r_{u2}, r_{u3} (being the normal distances from the centerline) positioned by two variable ratios, D_1 and D_3, along the centerline with the middle ratio, D_2, fixed at 0.5; and five for the lower wall r_{l1}, r_{l2}, r_{l3} (being the distances along the lines intersecting the centerline) defined by two variables ϕ_1 and ϕ_3 with ϕ_2 fixed at 45 deg.

B. Results

Figure 7 shows the development of the optimization process using this parameterization, showing C_p values for design points 1 to 200 representing the initial 200 DoE points, design points 201 through 300 representing the subsequent update points and the final 301 to 350 design points from the 50-point local exploration in 20% of the design space. The bold line indicates the current best optimum as each update point was added. We have adhered to the convention of performing roughly 10 times as many experiments as design variables to cover the design space sufficiently within the initial DoE. Despite mentioning earlier that the minimum number of updates is generally at least twice the number of points used in the initial DoE, we have found that for a 16 design variable problem, large compute times are needed to construct a response surface with upwards of 200 points. For this reason, we have limited our updates to just 100 points.

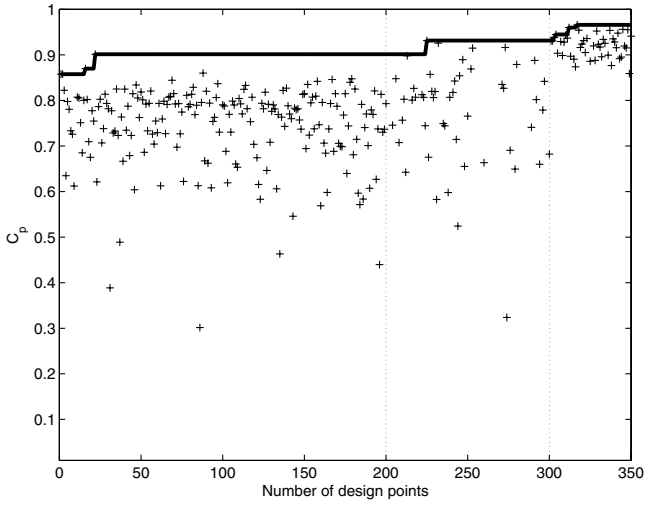

Fig. 7 Optimization history.

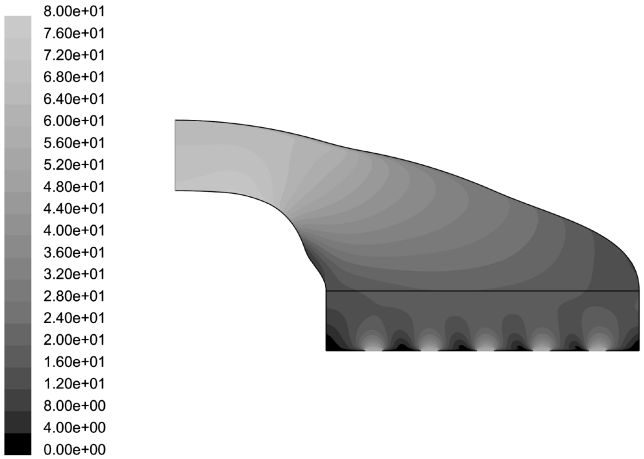

Fig. 8 Filled contours of velocity in a design found which contains no flow separation with $C_p = 0.7805$.

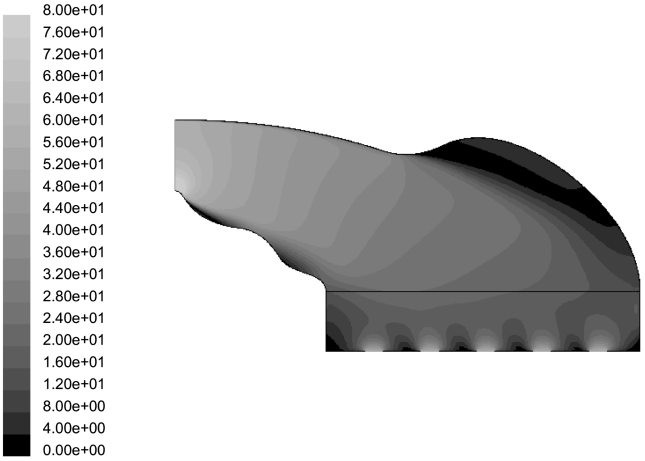

Fig. 9 Filled contours of velocity in the best design found having completed 100 update points with $C_p = 0.9316$.

A wide range of interestingly shaped diffusers were produced within the first 300 design points from convergent-divergent wall shapes to diffusers with one bulge feature on the lower wall and various bulges on the upper wall. Many designs, such as the convergent-divergent ones, contained no areas of separation. However, due to the increase in kinetic energy of the flow through the slight convergence the pressure recoveries were lower than the best value seen, the best ranging between $C_p = 0.7$ and $C_p = 0.8$. Designs that are similar to those seen within the actual race cars were also found within our design space, with straight upper walls to fit within the present design of roll bar structure, i.e., that had no radical geometric features such as bulges seen on either wall. One such airbox can be seen in Fig. 8. Again, we can see that separation has been completely eliminated. However, with a pressure recovery of $C_p = 0.7805$ it was significantly lower than the best design found. The best design had a pressure recovery of $C_p = 0.9316$ and is shown in Fig. 9. Here, completely different geometric features have emerged. Two small bulges have been formed along the lower wall inducing separation within these bulges, the bubbles of separation being completely contained within the bulges. The upper wall also contains a bulge within which forms another bubble of separation. It is important to note here that these bulges formed are not due to the case of rippling as described in Sec. V.A. Here, all three control points along the lower spline sit at the inflexion points of the curve and so the spline is not "overshooting" the point which is what leads to the rippling situation.

After 300 design points were tested, our process continued with a 50-point local exploration around the current best point found with $C_p = 0.9316$, reducing the range of each variable to 20% of the domain centered around this point. From Fig. 7 these are shown as

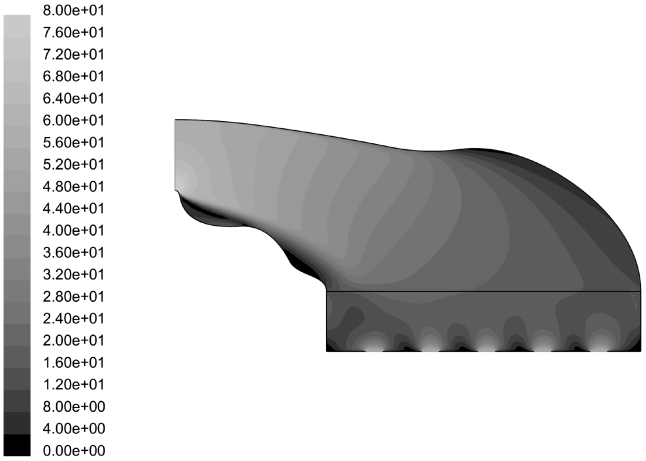

Fig. 10 Filled contours of velocity in the optimum design with $C_p = 0.9658$.

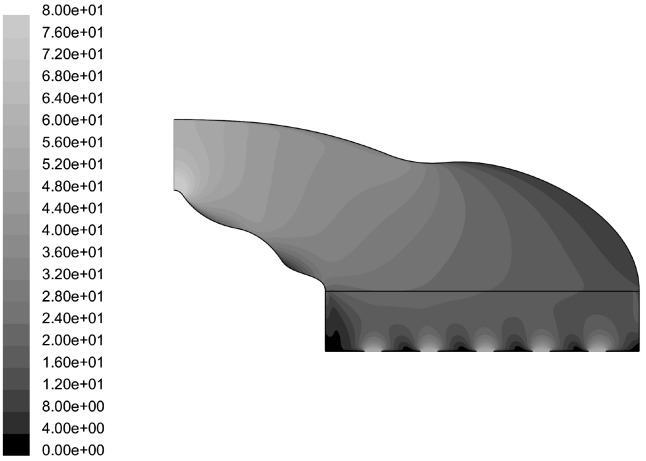

Fig. 11 Filled contours of velocity in a design which contains no separation with $C_p = 0.9452$.

design points 301–350. It is clear that by focusing on a small region within such a large design space and by performing a dense search in this area we can converge our model more quickly to a better design yielding a higher C_p value. Our optimum design was found with $C_p = 0.9658$ and is illustrated in Fig. 10. As we can see here, the upper bulge has been reduced slightly, eliminating separation on this wall. The lower bulges, however, remain present and capture small bubbles of separation within them. The upper and lower bounds of the whole design space, together with the design variable values for the best design after 300 design points and after the local exploration are shown in Table 1.

An interesting observation is that after the completion of the update points and analysis of the best design attained at that point, one could intuitively think that a better design could be achieved by eliminating separation, creating a design with walls following the flow streamlines of the airbox illustrated in Fig. 9. However, the subsequent local exploration has produced a design without separation different to that of following the streamlines of the airbox shown in Fig. 9. This airbox has a pressure recovery value $C_p = 0.9452$ and is shown in Fig. 11. If we followed the streamlines of the airbox in Fig. 9, the upper wall would have been straight. What we have seen is that by a small manipulation of the design variables, we can eliminate separation without following the streamlines of the best design after the update process to produce a design with a higher pressure recovery value. Another interesting design found within the local exploration returning a high pressure recovery value of $C_p = 0.9555$ is shown in Fig. 12. This airbox does feature a straight upper wall as well as two small bumps on the lower wall. This is of particular interest to the F1 aerodynamicist as this design would not require a redesign of the current roll bar structure in which the airbox sits.

We can see that for all the airboxes illustrated in Figs. 10–12, the elimination of separation on the upper wall is desired to return a high pressure recovery. It is also clear that the lower wall bulges are useful features in delivering an efficient expansion of the flow without experiencing losses from extensive separation. These bulges are allowed to exist due to the parameterization technique proposed, the key attribute of which is the geometric independence of the upper wall from the lower wall. Bulges containing small regions of separation have previously been seen to be beneficial in terms of reducing excessive nonuniformity of the flow at the diffuser exit when applied to a curved subsonic S-duct diffuser [7]. Increased losses in the airbox would occur from separation when the flow experiences excessive nonuniformity of the flow through the filter. This is not the case here as the small separation bubbles are completely contained within the lower wall bumps. In this study, we see a benefit of the two bulges containing small separation bubbles returning a higher pressure recovery over that of a design which eliminates separation entirely. It is clear that the balance between the size of bump on the upper wall and size of bumps on the lower wall, which together control the expansion of the flow as it turns, is very fine. This balance has been explored computationally through the capability of the parameterization technique proposed as it has strong local control. However, we would accept that there is a need for further research into such features including experimental testing due

Table 1 Design parameters and their corresponding bounds with the variable values for the best design found after 100 update points and again after a further 50 point local exploration

Variable	Lower bound	Upper bound	Best value after update	Best value after local exploration
CP1x	0.1	0.175	0.1408	0.1399
CP1y	−0.015	0	−0.0122	−0.0120
CP2x	0.25	0.325	0.2501	0.2481
CP2y	−0.08	0	−0.0675	−0.0685
CP3x	0.375	0.55	0.4181	0.4290
CP3y	−0.202	−0.09	−0.2018	−0.1920
Upper x ratio 1	0.05	0.45	0.1853	0.1703
Upper x ratio 2	0.5	0.5	0.5	0.5
Upper x ratio 3	0.55	0.9	0.6162	0.5943
r_{u1}	0.055	0.08	0.0651	0.0673
r_{u2}	0.07	0.14	0.1359	0.1333
r_{u3}	0.145	0.28	0.2128	0.2111
ϕ_1	5	40	17.9152	18.3529
ϕ_2	45	45	45	45
ϕ_3	50	85	84.8928	83.5803
r_{l1}	−0.08	−0.055	−0.0734	−0.0712
r_{l2}	−0.14	−0.07	−0.1295	−0.1234
r_{l3}	−0.2	−0.15	−0.1506	−0.1462
Pressure recovery			0.9316	0.9658

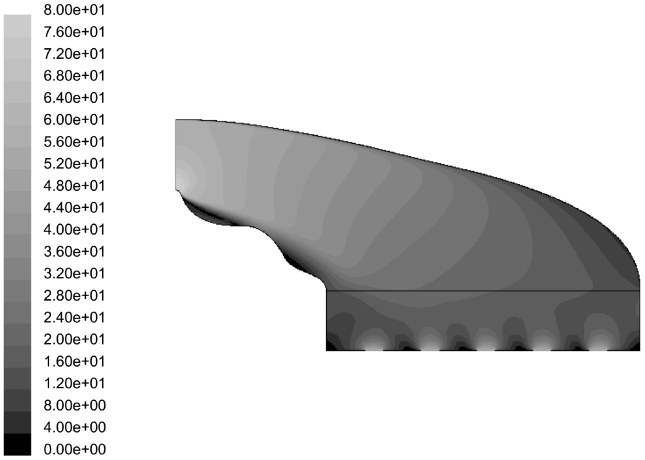

Fig. 12 Filled contours of velocity in a design with a straight upper wall and $C_p = 0.9555$.

to the uncertainty accompanying accurate prediction of separation and reattachment using RANS solvers.

VIII. Concluding Remarks

We have approached the design optimization of a two-dimensional F1 airbox by breaking down the expanding turning duct into its separate features. Using the knowledge gained through studying varying geometry parameterization techniques to design a straight diffuser and a constant width turning elbow, we have fused the best ideas from each to form a flexible parameterization technique that models a two-dimensional turning diffuser. The resulting parameterization approach for the 2-D airbox has uncoupled upper and lower walls, offering strong local geometric control. This in turn increases the design variable count, but, by applying a sophisticated response surface based optimization strategy using Kriging, we can efficiently optimize such a high dimensional problem. Although the number of update points that can be calculated is related to the compute power available, once the computational limit has been reached for building the response surface models we can conclude the update process and perform a local exploration around the current best point. This has allowed us to converge the model quickly to find small changes to the design which will yield higher pressure recovery values.

Such a two-stage search process coupled with a parametric geometry offering strong local control has allowed us to efficiently obtain superior designs that are nonintuitive to a designer.

References

[1] Patterson, G. N., "Modern Diffuser Design," *Aircraft Engineering*, Vol. 10, Sept. 1938, pp. 267–273.

[2] *2005 Formula One Technical Regulations*, Federation Internationale de L'Automobile, 2005.

[3] Myers, R. H., and Montgomery, D. C., *Response Surface Methodology: Process and Produce Optimization Using Design of Experiments*, Wiley, New York, 1995.

[4] Jones, D. R., Schonlau, M., and Welch, W. J., "Efficient Global Optimization of Expensive Black-Box Functions," *Journal of Global Optimization*, Vol. 13, No. 4, 1998, pp. 455–492.

[5] Mead, R., *The Design of Experiments*, Cambridge Univ. Press, Cambridge, England, U.K., 1988.

[6] Alexandrov, N., Dennis, J. E., Lewis, R. M., and Torczon, V., "A Trust Region Framework for Managing the Use of Approximation Models in Optimization," *Structural Optimization*, Vol. 15, No. 1, 1998, pp. 16–23.

[7] Zhang, W.-L., Knight, D. D., and Smith, D., "Automated Design of a Three-Dimensional Subsonic Diffuser," *Journal of Propulsion and Power*, Vol. 16, No. 6, 2000, pp. 1132–1140.

[8] Samareh, J. A., "A Survey of Shape Parameterization Techniques," NASA CP-1999-209136, June 1999, pp. 333–343.

[9] Braibant, V., and Fleury, C., "Shape Optimal Design Using B-Splines," *Computer Methods in Applied Mechanics and Engineering*, Vol. 44, Aug. 1984, pp. 247–267.

[10] Farin, G., *Curves and Surfaces for Computer Aided Geometric Design*, Academic Press, New York, 1990.

[11] Hicks, R. M., and Henne, P. A., "Wing Design by Numerical Optimization," *Journal of Aircraft*, Vol. 15, No. 7, July 1978, pp. 407–412.

[12] "CFD Flow Modeling Software," Fluent, Sheffield, U.K., 2005, www.fluent.com.

[13] Launder, B. E., and Spalding, D. B., "The Numerical Computation of Turbulent Flows," *Computer Methods in Applied Mechanics and Engineering*, Vol. 3, No. 2, 1974, pp. 269–289.

[14] Spalart, P. R., and Allmaras, S. R., "A One-Equation Turbulence Model for Aerodynamic Flows," AIAA Paper 92-0439, Jan. 1992.

[15] *Fluent User Guide*, Fluent, Sheffield, U.K., 2003.

[16] Keane, A. J., *The Options Design Exploration System Reference Manual and User Guide—Version B3.1*, Southampton, England, U.K., http://www.soton.ac.uk/~ajk/options.ps, 2002.

[17] Sobol, I. M., "On the Systematic Search in a Hypercube," *SIAM Journal on Numerical Analysis*, Vol. 16, No. 5, 1979, pp. 790–793.

[18] Statnikov, R. B., and Matusov, J. B., *Multicriteria Optimization and Engineering*, Chapman and Hall, New York, 1995.

[19] Sóbester, A., Leary, S. J., and Keane, A. J., "On the Design of Optimization Strategies Based on Global Approximation Models," *Journal of Global Optimization*, Vol. 33, No. 1, 2005, pp. 31–59.

[20] Sacks, J., Welch, W. J., Mitchell, T. J., and Wynn, H. P., "Design and Analysis of Computer Experiments," *Statistical Science*, Vol. 4, No. 4, 1989, pp. 409–435.

[21] Cressie, N., "The Origins of Kriging," *Mathematical Geology*, Vol. 22, No. 3, 1990, pp. 239–252.

[22] Keane, A. J., "Wing Optimization Using Design of Experiment, Response Surface and Data Fusion Methods," *Journal of Aircraft*, Vol. 40, No. 4, 2003, pp. 741–750.

[23] Jones, D. R., "A Taxonomy of Global Optimization Based on Response Surfaces," *Journal of Global Optimization*, Vol. 21, No. 4, 2001, pp. 345–383.

[24] Yuret, D., and de la Maza, M., "Dynamic Hill Climbing: Overcoming the Limitations of Optimization Techniques," *Proceedings of the 2nd Turkish Symposium on AI and ANN*, 1993, pp. 254–260, http://home.ku.edu.tr/dyuret/pub/tainn93.html.

[25] Kline, S. J., Abbott, D. E., and Fox, R. W., "Optimum Design of Straight-Walled Diffusers," *Journal of Basic Engineering*, Vol. 81, No. 3, 1959, pp. 321–331.

[26] Fox, R. W., and Kline, S. J., "Flow Regimes in Curved Subsonic Diffusers," *Journal of Basic Engineering*, Vol. 84, Sept. 1962, pp. 303–316.

[27] Reneau, L. R., "Performance and Design of Straight, Two-Dimensional Diffusers," *Journal of Basic Engineering*, March 1967, pp. 141–150.

[28] Carlson, J. J., Johnston, J. P., and Sagi, C. J., "Effects of Wall Shape on Flow Regimes and Performance in Straight Two-Dimensional Diffusers," *Journal of Basic Engineering*, March 1967, pp. 151–160.

[29] Glowinski, R., and Pironneau, O., "On the Numerical Computation of the Minimum-Drag Profile in Laminar Flow," *Journal of Fluid Mechanics*, Vol. 72, No. 2, 1975, pp. 385–389.

[30] Zhang, J., Chu, C. K., and Modi, V., "Design of Plane Diffusers in Turbulent Flow," *Inverse Problems in Engineering*, Vol. 2, March 1995, pp. 85–102.

[31] Lim, S., and Choi, H., "Optimal Shape Design of a Two-Dimensional Asymmetric Diffuser in Turbulent Flow," *AIAA Journal*, Vol. 42, No. 6, 2004, pp. 1154–1169.

[32] Madsen, J. I., Olhoff, N., and Condra, T. J., "Optimization of Straight, Two-Dimensional Diffusers by Wall Contouring and Guide Vane Insertion," *Proceedings of 3rd World Congress on Structural and Multidisciplinary Optimization*, edited by C. Bloebaum, Buffalo, NY, 1999, pp. 629–631.

[33] Ghate, D., Isaacs, A., Sudhakar, K., Mujumdar, P. M., and Marathe, A. G., "3d-Duct Design Using Variable Fidelity Method," AIAA Paper 2004-4427, Sept. 2004.

[34] Sóbester, A., and Keane, A. J., "Empirical Comparison of Gradient-Based Methods on an Engine-Inlet Shape Optimization Problem," AIAA Paper 2002-5507, 2002.

[35] Madsen, J. I., Shyy, W., and Haftka, R. T., "Response Surface Techniques for Diffuser Shape Optimization," *AIAA Journal*, Vol. 39, No. 9, 2000, pp. 1512–1518.

[36] Bezier, P. E., *Emploi des Machines a Commande Numerique*, Masson et Cie., Paris, 1970.

A. Messac
Associate Editor